J|A|C|S
ARTICLES
Published on Web 01/04/2007

Synthesis, Structure, and Magnetic Properties of an Antiferromagnetic Spin-Ladder Complex: Bis(2,3-dimethylpyridinium) Tetrabromocuprate

Alexander Shapiro,[†] Christopher P. Landee,[†] Mark M. Turnbull,*[,‡] Joaquim Jornet,[§] Mercè Deumal,[§] Juan J. Novoa,*[,§] Michael A. Robb,[||] and William Lewis[⊥]

Contribution from the Department of Physics and Carlson School of Chemistry and Biochemistry, Clark University, 950 Main Street, Worcester, Massachusetts 01610, Departament de Química Física, Facultat de Química, and CeRQT, Universitat de Barcelona, Martí i Franquès 1, 08028-Barcelona, Spain, Department of Chemistry, Imperial College London, South Kensington Campus, SW7 2AZ London, U.K., and Department of Chemistry, University of Canterbury, Private Bag 4800, Christchurch, New Zealand

Received September 1, 2006; E-mail: mturnbull@clarku.edu

Abstract: The complex $(2,3\text{-dmpyH})_2CuBr_4$ has been synthesized and its crystal packing determined by single-crystal X-ray diffraction (2,3-dmpyH = 2,3-dimethylpyridinium). The compound crystallizes in the triclinic space group $P\bar{1}$. The crystal packing is characterized by the formation of a ladder structure for the $CuBr_4$ anions showing short Br···Br contacts. The rungs of the ladder are formed via a crystallographic inversion center, while the rails are formed via unit cell translations. Variable temperature magnetic susceptibility measurements agree very well with the ladder model [$J_{rung} = -3.10$ cm^{-1} (-4.34 K) and $J_{rail} = -6.02$ cm^{-1} (-8.42 K)]. The assignment as a magnetic ladder is confirmed by first principles bottom-up theoretical calculations which conclude that $J_{rung} = -3.49$ cm^{-1} (-4.89 K) and $J_{rail} = -7.79$ cm^{-1} (-10.9 K), in very good agreement with the experimental values. They also support the absence of additional significant magnetic exchange within the crystals. Thus, $(2,3\text{-dmpyH})_2CuBr_4$ represents the second reported example of a weak-exchange limit magnetic ladder (that is, one in which the exchange along the rail is stronger than that across the rung).

Introduction

The study of low-dimensional molecular magnetic lattices has become prominent over the past several decades.[1−3] Magnetic ladders consist of two identical magnetic chains (with intrachain J_{rail} interaction) linked together by bridging units (J_{rung} interaction); there are no interactions between *ideal* ladders. Such ladders have been a special topic of interest owing to the presence of an energy gap in the spin excitation spectrum of even-leg ladders[4,5] and to their connection to other gapped systems[3] including $S = 1$ Haldane chains.[6] Under certain conditions, ladders have been shown to undergo a transition to a superconducting phase[7,8] and to play a role in certain phases of high-temperature superconductors.[9]

Among the best studied ladders are the copper oxide derived systems.[4,8,10−12] However, the very strong exchange observed in these materials makes it difficult to study them in their disordered state, or in applied fields that constitute a significant fraction of either the lower or upper critical fields. Molecular magnetic systems, on the other hand, have the advantage of weaker interactions, which allows experiments in all regions of the magnetic excitation spectrum. These systems also are more readily adjusted through tuning of the ancillary portions of the structure, allowing for tuning of the interactions with respect to both the strength and sign of the magnetic exchange.

A small number of purely organic magnets with probable ladder structures have been reported[13−16] along with a family of hybrid metal−organic compounds which derived their

[†] Department of Physics, Clark University.
[‡] Carlson School of Chemistry and Biochemistry, Clark University.
[§] Universitat de Barcelona.
[||] Imperial College London.
[⊥] University of Canterbury.

(1) Girtu, M. A. *Magn. Nanostruct.* **2002**, 359−405.
(2) Dagotto, E. *Rep. Prog. Phys.* **1999**, *62*, 1525.
(3) Bose, I. *Curr. Sci.* **2005**, *88* (1), 62−70.
(4) Schmidt, K. P.; Uhrig, G. S. *Mod. Phys. Lett. B* **2005**, *19* (24), 1179−1205.
(5) Dagotto, E.; Rice, T. M. *Science (Washington, DC)* **1996**, *271* (5249), 618−623.
(6) White, S. R. *Phys.l Rev. B: Condens. Matter Mater. Phys.* **1996**, *53* (1), 52.
(7) Uehara, M.; Nagata, T.; Akimitsu, J.; Takahashi, H.; Mori, N.; Kinoshita, K. *J. Phys. Soc. Jpn.* **1996**, *65* (9), 2764−2767.
(8) Nakanishi, T.; Motoyama, N.; Mitamura, H.; Takeshita, N.; Takahashi, H.; Eisaki, H.; Uchida, S.; Mori, N. *Phys. Rev. B: Condens. Matter Mater. Phys.* **2005**, *72* (5), 054520/1−054520/6.
(9) Tranquada, J. M.; Woo, H.; Perring, T. G.; Goka, H.; Gu, G. D.; Fujita, M.; Yamada, K. *Nature (London)* **2004**, *429*, 534.
(10) Vuletic, T.; Korin-Hamzic, B.; Ivek, T.; Tomic, S.; Gorshunov, B.; Dressel, M.; Akimitsu, J. *Phys. Rep.* **2006**, *428* (4), 169−258.
(11) Carter, S. A.; Batlogg, B.; Cava, R. J.; Krajewski, J. J.; Peck, W. F., Jr.; Rice, T. M. *Phys. Rev. Lett.* **1996**, *77* (7), 1378−1381.
(12) Azuma, M.; Hiroi, Z.; Takano, M.; Ishida, K.; Kitaoka, Y. *Phys. Rev. Lett.* **1994**, *73* (25), 3463−3466.
(13) Yoshida, Y.; Tateiwa, N.; Mito, M.; Kawae, T.; Takeda, K.; Hosokoshi, Y.; Inoue, K. *Phys. Rev. Lett.* **2005**, *94* (3), 037203/1−037203/4.
(14) Kikuchi, M.; Okamoto, K.; Okunishi, K.; Sakai, T. *Prog. Theor. Phys. Suppl.* **2005**, *159*, 251−255.

10.1021/ja066330m CCC: $37.00

magnetic properties from the organic component.[17,18] A somewhat larger number of coordination compounds have been reported which exhibit magnetic-ladder behavior and owe the source of the magnetic moment to the metal species. These include several copper(II) complexes in which the ladder motif results from crystal packing of CuX_4^{2-} ions,[19−22] as well as those where the ladder structure results from bridging diamagnetic ligands.[23−25]

Recent experience shows that the magnetic behavior of a compound may be more complex than first suggested by knowledge of the crystal structure. The dominant interactions may occur in directions different than those showing the shortest inter-radical distances and/or the interladder interactions may not be negligible. The vanadium compound $(VO)_2(P_2O_7)$ has been studied extensively and was originally interpreted as a two-leg magnetic ladder.[26−28] However, subsequent neutron scattering experiments showed that the principal magnetic interactions were those of an alternating chain oriented perpendicular to the structural ladder motif.[29,30] Other problems result when the symmetry of the system is lower than that of the ideal ladder with only the rail and rung exchange pathways. The copper complex Cu_2(1,4-diazacycloheptane)Cl_4 was reported and studied as a magnetic ladder,[25,31−33] but subsequent studies indicated that the system is more complex and that the application of a ladder Hamiltonian is an oversimplification.[34,35]

We have been interested in designing a series of magnetic ladders in both the limiting cases of strong rung exchange and strong rail exchange as well as isotropic systems. Thus, we have prepared a number of systems which appear structurally as two-leg ladders and whose magnetic behavior agrees with that analysis using both the crystal-packing and bridging-ligand techniques.[19,21,23,24,36] In the case of an isotropic magnetic ladder, properties have also been rationalized at the theoretical level.[19] We report here the synthesis, structure, magnetic susceptibility, and theoretical model of the new strong rail ladder (2,3-dmpyH)$_2$CuBr$_4$ [2,3-dmpyH = 2,3-dimethylpyridinium].

Experimental

2,3-Dimethylpyrazine was purchased from Aldrich and used as received. Copper(II) bromide was purchased from Aesar and used as received. IR spectra were recorded on a Perkin-Elmer Paragon 500 spectrophotometer and referenced to polystyrene.

Bis(2,3-dimethylpyridinium) Tetrabromocuprate(II) [(2,3-dmpyH)$_2$CuBr$_4$] 1. Copper(II) bromide (2.172 g, 9.72 mmol) was dissolved in 30 mL of water, resulting in a bluish green mixture which was filtered to remove traces of insoluble material. Aqueous HBr (21.6 mL of 9 M) was added to 2,3-dmpy (2.084 g, 19.4 mmol) giving a pale-orange solution. The solution of (2,3-dmpyH)Br was added slowly to the stirring $CuBr_2$ solution resulting in a dark red/black solution. The solution was then placed in a desiccator. Crystal formation was observed after about three weeks, and the first crystals were harvested after five weeks. The majority of the solution was decanted and the crystals were then filtered and washed with *tert*-butanol, while the decanted solution was placed back in the desiccator. The harvesting procedure was repeated four times, resulting in a combined product of 4.66 grams (80%). The crystals were dark red/purple, essentially opaque, and shaped as elongated rectangular prisms and parallelepipeds.

X-ray Diffraction. A crystal of **1** was mounted on a glass fiber using a fluorocarbon oil. Data was collected at 88(2) K using a Bruker/Siemens SMART system (Mo Kα radiation, $\lambda = 0.71073$) using φ and ω scans. The first 50 frames were recollected at the end of the data collection to monitor for decay. Cell parameters were determined using SMART[37] software and refined using SAINTPlus.[38] Data reduction and corrections were performed using SAINTPlus.[38] Absorption corrections were made via SADABS.[39] The structure was solved via direct methods using SHELXS97[40] and refined via least-squares using SHELXL97.[41] Crystallographic details are given in Table 1. Selected bond lengths and angles are given in Tables 2 and 3. The structure has been deposited with the CCDC (CCDC No. 607284). A Bruker D8 powder X-ray diffractometer was used to verify that powder samples used for magnetic measurements were the same phase as the single crystal.

Magnetic Data Collection. Data were collected using a Quantum Design MPMS-XL SQUID magnetometer. Crystals of **1** were powdered and packed into a no. 3 gelatin capsule. The magnetization of the sample as a function of applied field was collected from 0 to 50 kOe at 1.8 K; no hysteresis was observed. Susceptibility data were taken over the temperature range from 1.8 to 325 K in an applied field of 1 kOe.

Computational Details. A theoretical study of the magnetic interactions of this crystal was performed using a first-principles *bottom-*

(15) Sakai, T.; Okamoto, K.; Okunishi, K.; Kindo, K.; Narumi, Y.; Hosokoshi, Y.; Katoh, K.; Inoue, K.; Goto, T. *Physica B (Amsterdam)* **2004**, *346−347*, 34−37.
(16) Tamura, M.; Hosokoshi, Y.; Shiomi, D.; Kinoshita, M.; Nakasawa, Y.; Ishikawa, M.; Sawa, H.; Kitazawa, T.; Eguchi, A.; Nishio, Y.; Kajita, K. *J. Phys. Soc. Jpn.* **2003**, *72* (7), 1735−1744.
(17) Ribas, X.; Mas-Torrent, M.; Perez-Benitez, A.; Dias, J. C.; Alves, H.; Lopes, E. B.; Henriques, R. T.; Molins, E.; Santos, I. C.; Wurst, K.; Foury-Leylekian, P.; Almeida, M.; Veciana, J.; Rovira, C. *Adv. Funct. Mater.* **2005**, *15* (6), 1023−1035.
(18) Wesolowski, R.; Haraldsen, J. T.; Musfeldt, J. L.; Barnes, T.; Mas-Torrent, M.; Rovira, C.; Henriques, R. T.; Almeida, M. *Phys. Rev. B: Condens. Matter Mater. Phys.* **2003**, *68* (13), 134405/1−13440.5/8.
(19) Deumal, M.; Giorgi, G.; Robb, M. A.; Turnbull, M. M.; Landee, C. P.; Novoa, J. J. *Eur. J. Inorg. Chem.* **2005**, (23), 4697−4706.
(20) Watson, B. C.; Kotov, V. N.; Meisel, M. W.; Hall, D. W.; Granroth, G. E.; Montfrooij, W. T.; Nagler, S. E.; Jensen, D. A.; Backov, R.; Petruska, M. A.; Fanucci, G. E.; Talham, D. R. *Phys. Rev. Lett.* **2001**, *86* (22), 5168−5171.
(21) Landee, C. P.; Turnbull, M. M.; Galeriu, C.; Giantsidis, J.; Woodward, F. M. *Phys. Rev. B: Condens. Matter Mater. Phys.* **2001**, *63* (10), 100402/1−10040.2/4.
(22) Willett, R. D.; Galeriu, C.; Landee, C. P.; Turnbull, M. M.; Twamley, B. *Inorg. Chem.* **2004**, *43* (13), 3804−3811.
(23) Wells, B. M.; Landee, C. P.; Turnbull, M. M.; Awwadi, F. F.; Twamley, B. *J. Mol. Catal. A: Chem.* **2005**, *228* (1−2), 117−123.
(24) Landee, C. P.; Delcheva, A.; Galeriu, C.; Pena, G.; Turnbull, M. M.; Willett, R. D. *Polyhedron* **2003**, *22* (14−17), 2325−2329.
(25) Chiari, B.; Piovesana, O.; Tarantelli, T.; Zanazzi, P. F. *Inorg. Chem.* **1990**, *29* (6), 1172−1176.
(26) Johnston, D. C.; Johnson, J. W.; Goshorn, D. P.; Jacobson, A. J. *Phys. Rev. B: Condens. Matter Mater. Phys.* **1987**, *35* (1), 219−222.
(27) Barnes, T.; Riera, J. *Phys. Rev. B: Condens. Matter Mater. Phys.* **1994**, *50* (10), 6817−6822.
(28) Eccleston, R. S.; Barnes, T.; Brody, J.; Johnson, J. W. *Phys. Rev. Lett.* **1994**, *73* (19), 2626−2629.
(29) Garrett, A. W.; Nagler, S. E.; Barnes, T.; Sales, B. C. *Phys. Rev. B: Condens. Matter Mater. Phys.* **1997**, *55* (6), 3631−3635.
(30) Garrett, A. W.; Nagler, S. E.; Tennant, D. A.; Sales, B. C.; Barnes, T. *Phys. Rev. Lett.* **1997**, *79* (4), 745−748.
(31) Chaboussant, G.; Crowell, P. A.; Levy, L. P.; Piovesana, O.; Madouri, A.; Mailly, D. *Phys. Rev. B: Condens. Matter Mater. Phys.* **1997**, *55* (5), 3046−3049.
(32) Chaboussant, G.; Julien, M. H.; Fagot-Revurat, Y.; Levy, L. P.; Berthier, C.; Horvatic, M.; Piovesana, O. *Phys. Rev. Lett.* **1997**, *79* (5), 925−928.
(33) Weihong, Z.; Singh, R. R. P.; Oitmaa, J. *Phys. Rev. B: Condens. Matter Mater. Phys.* **1997**, *55* (13), 8052−8055.
(34) Hammar, P. R.; Reich, D. H. *J. Appl. Phys.* **1996**, *79* (8, Part 2A), 5392−5394.
(35) Hammar, P. R.; Reich, D. H.; Broholm, C.; Trouw, F. *Phys. Rev. B: Condens. Matter Mater. Phys.* **1998**, *57* (13), 7846−7853.
(36) Turnbull, M. M.; Galeriu, C.; Giantsidis, J.; Landee, C. P. *Mol. Cryst. Liq. Cryst. Sci. Technol., Sect. A* **2002**, *376*, 469−476.
(37) *SMART, Bruker Molecular Analysis Research Tool;* Bruker AXS: Madison, WI, 1997−1998.
(38) *SAINTPlus. Data Reduction and Correction Program;* Bruker AXS: Madison WI, 1999.
(39) Sheldrick, G. M. *SADABS, an empirical absorption correction program,* version 2.01; Bruker AXS Inc.: Madison, WI, 1999.
(40) Sheldrick, G. M. *SHELXS97 Program for the Solution of Crystal Structures;* University of Göttingen, Göttingen, Germany, 1997.
(41) Sheldrick, G. M. *SHELXL97 Program for the Refinement of Crystal Structures;* University of Göttingen, Göttingen, Germany, 1997.

Table 1. Crystal Data and Structure Refinement for **1**

empirical formula	$C_{14}H_{20}N_2CuBr_4$
fw	599.50
temp	88(2) K
cryst syst	monoclinic
space group	$P2(1)/n$
unit cell dimensions	$a = 7.5037(6)$ Å $b = 31.613(3)$ Å, $\beta = 98.972(2)°$ $c = 8.2016(7)$ Å
volume	1921.7(3) Å^3
Z	4
density (calcd)	2.072 Mg/m^3
abs coeff	9.448 mm^{-1}
cryst size	0.25 × 0.12 × 0.03 mm^3
θ range for data collection	2.58 to 26.45°
index ranges	$-9 \le h \le 9$, $-39 \le k \le 37$, $-10 \le l \le 10$
reflctns collected	16513
independent reflctns	3895 [$R_{int} = 0.0572$]
completeness to $\theta = 26.45°$	98.2%
abs correction	empirical
max and min transm	0.7481 and 0.2749
refinement method	full-matrix least-squares on F^2
data/restraints/params	3895/0/200
GOF on F^2	1.039
final R indices [$I > 2\sigma(I)$]	R1 = 0.0359, wR2 = 0.0672
R indices (all data)	R1 = 0.0573, wR2 = 0.0724

Table 2. Selected Bond Lengths [Å] and Angles [deg] for **1**[a]

Cu−Br1	2.4118(7)	Cu−Br2	2.3842(7)
Cu−Br3	2.3841(7)	Cu−Br4	2.3524(7)
Br1···Br2A	3.905(1)	Br3···Br3C	4.328(1)
Br1−Cu−Br2	98.61(2)	Br1−Cu−Br3	126.24(3)
Br1−Cu−Br4	102.25(3)	Br2−Cu−Br3	101.12(2)
Br2−Cu−Br4	130.60(3)	Br3−Cu−Br4	101.54(3)
Cu−Br1···Br2A	151.0(1)	Br1···Br2A−Cu2A	127.6(1)
Cu−Br3···Br3C	155.5(1)	Br3···Br3C−CuC	155.5(1)
Cu−Br1···Br2A−CuA	−2.0(1)	Cu−Br3···Br3C−CuC	180.0

[a] Symmetry transformations used to generate equivalent atoms: (A) $x + 1, y, z$; (C) $1 - x, -y, -z$.

up approach,[42] consisting of four steps: (1) analysis of the crystal structure to find all unique radical−radical pairs present in the crystal, (2) computation of the radical−radical magnetic interactions (J_{AB}) for each unique radical−radical pair found in the crystal, (3) determination of the magnetic topology of the crystal, and its minimal magnetic model space, and (4) calculation of the macroscopic magnetic properties of the crystal using the full energy spectrum obtained by diagonalization of the matrix representation of the appropriate Heisenberg Hamiltonian (the matrix representation is computed on the space of spin functions of the minimal magnetic model space). Such matrix representation is only a function of the J_{AB} parameters whose values were computed in step 2.

This approach is an objective four-step procedure for connecting the microscopic to the macroscopic magnetic information, with step 3 being the key step for such a micro-to-macro connection. We must stress the fact that this first-principles bottom-up procedure benefits from well-known theoretical methods from chemistry (step 2) and physics (step 4) as part of a global strategy to study molecular magnetism. It is *bottom-up* because the macroscopic magnetic properties are obtained from the microscopic radical−radical magnetic interactions using the crystal structure (cluster/periodic approach[42]) as the only input, that is, without making any starting assumptions about the nature or strength of the magnetic interactions established between the radicals of the crystal. It is also first-principles because the J_{AB} for each pair is

Table 3. Hydrogen Bonds for **1** [Å and deg][a]

D−H···A	d(D−H)	d(H···A)	d(D···A)	∠(DHA)
N1−H1···Br2#1	0.85(5)	2.53(5)	3.254(4)	144(4)
N1−H1···Br1#2	0.85(5)	2.98(5)	3.458(4)	118(4)
N11−H11···Br1	0.79(5)	2.63(5)	3.374(4)	159(5)

[a] Symmetry transformations used to generate equivalent atoms: (#1) $-x + 1, -y, -z + 2$; (#2) $-x, -y, -z + 2$.

obtained from the energy difference between the appropriate states computed by first-principles methods (accurate ab initio or DFT methods[42]). Once the J_{AB} values are known, we can diagonalize the corresponding Heisenberg Hamiltonian. We have used the following Heisenberg Hamiltonian, which is more convenient for our computer codes:

$$\hat{H} = -2 \sum_{A,B} J_{AB}(\hat{S}_A \cdot \hat{S}_B + (^1/_4)\, \hat{I}_{AB}) \quad (1)$$

where $\hat{I}_{AB}$ is the identity operator and $\hat{S}_A$ ($\hat{S}_B$) is the spin operator acting on radical A (B). The energy spectrum computed using this Hamiltonian results in the same energy differences between different eigenvalues as those obtained using the more common expression:

$$\hat{H} = -2 \sum_{A,B} J_{AB} \hat{S}_A \cdot \hat{S}_B \quad (2)$$

The energy spectra for these Hamiltonians are obtained by diagonalization of its matrix representation on the basis of spin-eigenfunctions of a finite model crystal that mimics the magnetic properties of the infinite crystal (the so-called *minimal magnetic model space*). This allows the rigorous computation of the macroscopic magnetic properties using the adequate statistical mechanics expressions.[42] The minimal magnetic model space is selected once the magnetic topology of the crystal is determined as part of the study in terms of the magnetic connectivity that the J_{AB} values define among the radicals. The minimal model space is formed by the smallest set of radicals whose extension along the three crystallographic axes reproduces such topology and, thus, the infinite crystal. Such space must include all significant J_{AB} interactions and in the same ratio as found in the infinite crystal. Furthermore, the macroscopic properties computed with finite spaces should converge toward the experimental data (which would theoretically correspond to the infinite crystal) as we enlarge the finite magnetic space.[42] Notice that the size of the matrix representation of the Heisenberg Hamiltonian increases with the number of doublet radical N centers as $N!/[(N/2)!(N/2)!]$. In practice, this means that we can reach up to 16 different doublet centers.

The only spin carrying units in the $(2,3\text{-dmpyH})_2CuBr_4$ crystal are the $CuBr_4^{2-}$ anions. Each $CuBr_4^{2-}$ unit is a doublet radical by means of the unpaired electron of the Cu(II), which does not belong entirely to the Cu(II) atom since it is also shared over the Br atoms owing to spin polarization. Therefore, only two states are possible for the A−B radical pairs: a singlet and a triplet state. The value of J_{AB} for each pair is thus obtained from the energy difference between the open-shell singlet and triplet states, both at the crystal geometry. We compute both energies using the B3LYP functional,[43−45] the Ahlrich-pVDZ[46] basis set for Cu, and a 6-31+G(d)[47,48] basis set for the remaining atoms. The broken symmetry approximation was used to compute the open-shell singlet for a proper description of its open-shell nature. Within

(42) Deumal, M.; Bearpark, M. J.; Novoa, J. J.; Robb, M. A. *J. Phys. Chem. A* **2002**, *106* (7), 1299−1315. (See references therein for in-depth discussion.)
(43) Becke, A. D. *Phys. Rev. A: At., Mol., Opt. Phys.* **1988**, *38* (6), 3098−3100.
(44) Lee, C.; Yang, W.; Parr, R. G. *Phys. Rev. B; Condens. Matter Mater. Phys.* **1988**, *37* (2), 785−789.
(45) Becke, A. D. *J. Chem. Phys.* **1993**, *98* (7), 5648−5652.
(46) Schafer, A.; Horn, H.; Ahlrichs, R. *J. Chem. Phys.* **1992**, *97*, 2751.
(47) Hariharan, P. C.; Pople, J. A. *Theor. Chim. Acta* **1973**, *28* (3), 213−222.
(48) Francl, M. M.; Pietro, W. J.; Hehre, W. J.; Binkley, J. S.; Gordon, M. S.; DeFrees, D. J.; Pople, J. A. *J. Chem. Phys.* **1982**, *77* (7), 3654−3665.

Scheme 1

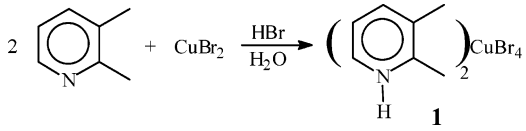

this approximation the value of J_{AB} for Hamiltonians (1) or (2) is obtained as $2J_{AB} = 2(E_{BS}^{S} - E^{T})$, where E^{T} is the energy of the triplet state and E_{BS}^{S} is the energy of the singlet state computed using the broken symmetry approach[49,50] (the expression for J_{AB} derives from the original broken-symmetry equations when the SOMO orbitals of the two radicals do not overlap, which is the usual situation in through-space magnetic interactions, such as those found in the (2,3-dmpyH)$_2$CuBr$_4$ crystal). Our experience indicates that this expression gives results closer to the experimental values than alternative ones where projection is used. It is worth pointing here that there has been some controversy about the use of projection when computing the values of the J_{AB} parameters using the broken-symmetry approach within the DFT context (for detailed discussions, see references 51 and 52). Also notice that when the expression for the Hamiltonian is

$$\hat{H} = -\sum_{A,B} J'_{AB}\hat{S}_A \cdot \hat{S}_B \qquad (3)$$

the values of the J'_{AB} thus obtained are equal to $2J_{AB}$ obtained with eqs 1 or (2).

The first-principles bottom-up procedure has been successfully applied to a series of crystals representative of a variety of macroscopic behaviors.[53−55] It connects the macroscopic magnetic properties with their microscopic origin (the J_{AB} values) in a numerically accurate and unbiased form. The only input required is the crystal geometry. No assumptions are made about the nature of the radical−radical interactions found in the crystal.

Results

Structure. Reaction of 2,3-dimethylpyridine with HBr and $CuBr_2$ in aqueous solution gave the salt (2,3-dmpyH)$_2$CuBr$_4$ (**1**) in 80% yield as nearly black crystals (Scheme 1). Crystals suitable for single-crystal X-ray diffraction grew directly from the solution through slow evaporation.

The compound crystallizes in the triclinic space group $P\bar{1}$, with two inversion related molecules in the unit cell. The asymmetric unit is shown in Figure 1. The $CuBr_4^{2-}$ anion is a distorted tetrahedron with Cu−Br bond lengths in the range 2.35−2.41 Å. The mean trans angle about the Cu is 128.42(4)°, smaller than is usually observed for tetrabromocuprate ions[56] but comparable with that seen in bis(4-methylpyridinium) tetrabromocuprate.[57] Bond lengths and angles within the two crystallographically independent 2,3-dimethylpyridinium ions compare well with each other and with previous results.[58,59]

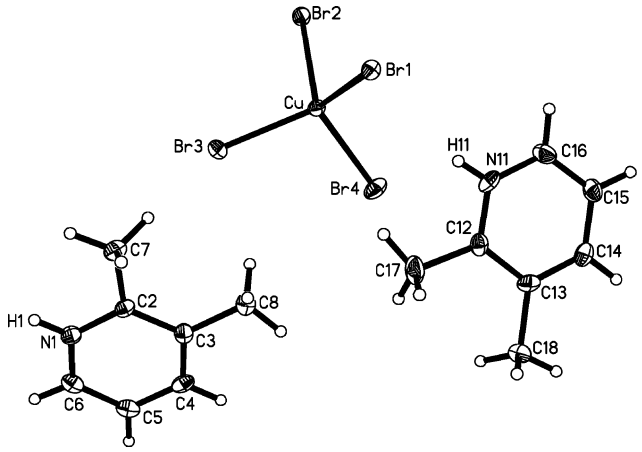

Figure 1. A plot of the asymmetric unit of **1** showing 50% probability ellipsoids. Only hydrogen atoms whose positions were refined are labeled.

From the structural point of view, nearest neighbor and next nearest neighbor contacts between bromine atoms in the crystal structure of **1** suggest that the $CuBr_4^{2-}$ radicals form a 2-leg spin-ladder (Figure 2a), with the ladders separated by the organic cations (Figure 2b). The rails of the ladder are formed via unit cell translations of the $CuBr_4^{2-}$ radicals parallel to the *a*-axis with a Br1···Br2A ($x + 1$, y, z) distance of 3.905(1) Å. The rungs of the ladder are formed by short contacts between inversion related $CuBr_4^{2-}$ ions with a Br3···Br3C ($1-x$, $-y$, $-z$) distance of 4.328(1) Å. The corresponding angles and torsion angles are given in Table 2.

The ladders are separated from each other by the organic cations (Figure 2b). The 2,3-dmpyH ions and $CuBr_4^{2-}$ ions form alternating layers parallel to the *ac*-plane, with the N1-containing 2,3-dmpyH rings and the N11-containing 2,3-dmpyH rings in separate layers. The layers alternate in the pattern $CuBr_4^{2-}$−N11 rings−$CuBr_4^{2-}$−N1 rings−$CuBr_4^{2-}$−N11 rings. The different packing motifs of the 2,3-dmpyH rings explain the ladder structure for the $CuBr_4^{2-}$ ions. The N11-containing rings are canted with respect to each other; the angle between rings is nearly 21°. This canting, and the interleaving of the methyl groups, forces the rings further apart parallel to the *b*-axis, resulting in nonbonding Br···Br distances larger than 6 Å, effectively isolating the ladders in that direction. The rings containing N1 are stacked parallel to the *a*-axis with alternating π-stacking interactions. Successive rings show alternating distances of 3.47(1) and 3.30(1) Å with displacement angles (defined as the angle between the normal to the mean plane of the ring and the line connecting the ring centroids) of 25.4° and 35.2°. Closer Br···Br contacts between ladders are observed parallel to the *c*-axis at 4.748(1) Å (see Figure 2b). These distances are small enough that there could be some magnetic exchange between ladders.

Susceptibility Measurements. The magnetization of **1** was collected as a function of field from 0 to 50 kOe at 1.8 K. The response was linear to 5 kOe and then showed distinct upward curvature to 50 kOe, characteristic of low-dimensional magnetic systems. Magnetic susceptibility data were collected as a function of temperature in a 1 kOe applied field from 1.8 to 325 K (Figure 3). The data show a broad rounded maximum at

(49) Noodlemann, L. *J. Chem. Phys.* **1981**, *74*, 5737.
(50) Noodlemann, L. *Chem. Phys.* **1986**, *109*, 131.
(51) Ruiz, E.; Alvarez, S.; Cano, J.; Polo, V. *J. Chem. Phys.* **2005**, *123*, 164110.
(52) Adamo, C.; Barone, V.; Bencini, A.; Broer, R.; Filatov, M.; Harrison, N. M.; Illas, F.; Malrieu, J. P.; Moreira, I. d. P. R. *J. Chem. Phys.* **2006**, *124*, 107101.
(53) Deumal, M.; Bearpark, M. J.; Robb, M. A.; Pontillon, Y.; Novoa, J. J. *Chem.—Eur. J.* **2004**, *10* (24), 6422−6432.
(54) Deumal, M.; Mota, F.; Bearpark, M. J.; Robb, M. A.; Novoa, J. J. *Mol. Phys.* **2006**, *104*, 857.
(55) Jornet, J.; Deumal, M.; Ribas-Arino, J.; Bearpark, M. J.; Robb, M. A.; Hicks, R. G.; Novoa, J. J. *Chem.−Eur. J.* **2006**, *12*, 3995.
(56) Turnbull, M. M.; Landee, C. P.; Wells, B. M. *Coord. Chem. Rev.* **2005**, *249* (23), 2567−2576.
(57) Luque, A.; Sertucha, J.; Castillo, O.; Roman, P. *New J. Chem. (Nouv. J. Chim.)* **2001**, *25*, 1208.
(58) Haynes, D. A.; Jones, W.; Motherwell, W. D. S. *Cryst. Eng. Commun.* **2005**, *7*, 538.
(59) Harada, A.; Tsuchimoto, M.; Ohba, S.; Iwasawa, K.; Tokii, T. *Acta Crystallogr., Sect. B: Struct. Sci.* **1997**, *53*, 654.

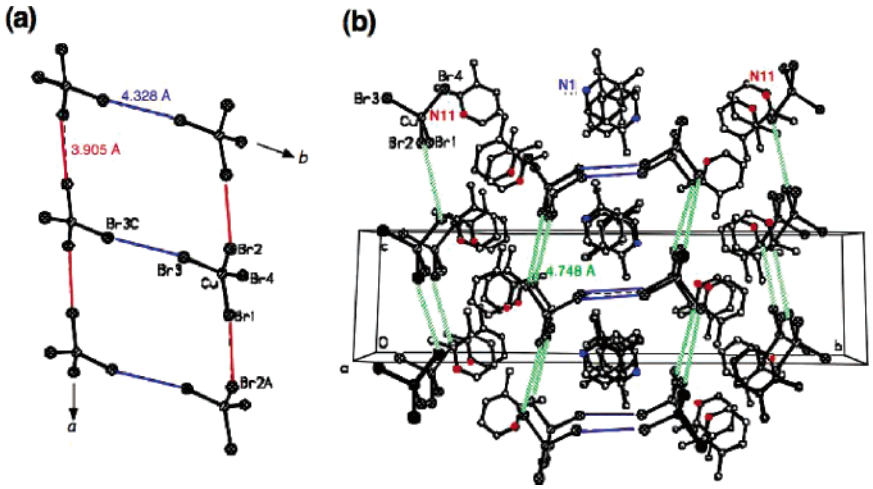

Figure 2. (a) Packing diagram of **1** showing the ladder structure of the $CuBr_4^{2-}$ anions, where rails and rungs are drawn along *a*- and *b*-axes, respectively (viewed parallel to the *c*-axis). (b) Packing diagram of **1** shows the isolation of the ladders viewed parallel to the *a*-axis. Blue lines show the short Br···Br contacts of the rungs while the green lines indicate the shortest interladder distance (4.748(1) Å). (H-atoms have been removed for clarity.)

11 K and decrease rapidly toward zero at lower temperatures. The maximum is characteristic of a low-dimensional Heisenberg antiferromagnet while the rapid decrease is due to the presence of a singlet ground state separated by an energy gap Δ from the first excited state. The data were fit to the strong-rail exchange model for a magnetic ladder using eq

$$F(T, C, J_{rung}, J_{rail}, P) = \frac{C \exp\left(\dfrac{-\Delta\left[\dfrac{J_{rung}}{J_{rail}}\right]}{\dfrac{T}{J_{rail}}}\right)}{T} \frac{1 + \left[\sum_{i=1}^{6}\left(\dfrac{J_{rail}}{T}\right)^i \sum_{j=0}^{3} N_{i,j}\left(\dfrac{J_{rung}}{J_{rail}}\right)^j\right]}{1 + \left[\sum_{i=1}^{6}\left(\dfrac{J_{rail}}{T}\right)^i \sum_{j=0}^{3} D_{i,j}\left(\dfrac{J_{rung}}{J_{rail}}\right)^j\right]} + \frac{PC}{T} \quad (4)$$

where $N_{i,j}$ and $D_{i,j}$ coefficients were determined mathematically,[60] *P* is the percent paramagnetic impurity, $\Delta(\alpha) = 0.4030\alpha + 0.0989\alpha^3$, α is the ratio J_{rung}/J_{rail}, and the Hamiltonian is $\hat{H} = \sum J'_{AB}\hat{S}_A \cdot \hat{S}_B$.[60] The best-fit parameters were $J'_{rail} = 16.85$ K (12.04 cm^{-1}), $J'_{rung} = 8.68$ K (6.2 cm^{-1}) and $P = 0.065\%$. Attempts to fit the data to the strong-rung exchange model gave parameters with no physical meaning.[60] In order to compare J' fitting parameters from eq 4 and J_{AB} from eqs 1 and 2, J'_{rail} and J'_{rung} must be translated as $-J'/2$ resulting in −8.42 K (−6.02 cm^{-1}) and −4.34 K (−3.10 cm^{-1}), respectively.

Theoretical Calculations. We applied our four-step, first-principles, *bottom-up* procedure with the following results. In the first step, using the 88(2) K crystal structure, we selected all unique radical−radical pairs with the potential to present non-negligible magnetic interactions. In practical terms, this selection was done by choosing those radical-pairs whose Cu···Cu distance is smaller than a cutoff of 10.0 Å (we checked that this cutoff includes all first and the closest second nearest neighbors, see Figure 4a). Given the already known exponential decrease with distance of the magnetic interactions, we are confident that we have included all relevant radical pairs. The five unique $CuBr_4^{2-}\cdots CuBr_4^{2-}$ pairs found (d1−d5) are shown in Figure 4b.

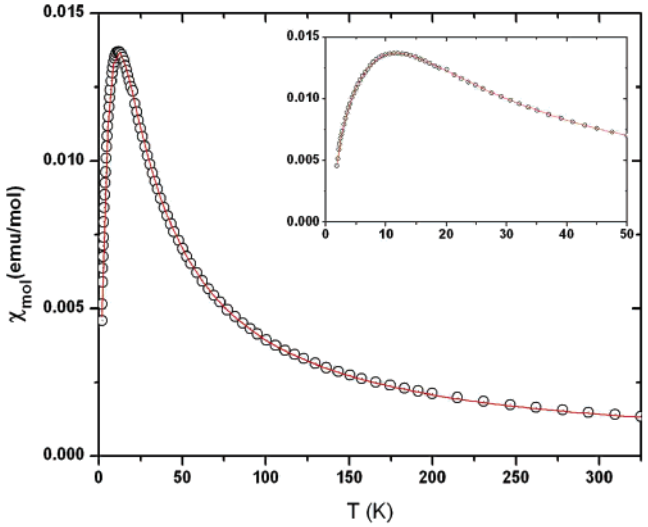

Figure 3. Magnetic susceptibility as a function of temperature for compound **1**. The open circles are the data and the line represents the best fit to a strong-rail exchange magnetic ladder model. The inset is an expansion of the region from 1.8 to 50 K.

The value of J_{AB} for each of these five pairs was then computed (step 2) for the *isolated* anion-pairs. As shown in Table 4, only three parameters are non-negligible: $J(d1) = -22.5$ cm^{-1}, $J(d2) = -0.22$ cm^{-1} and $J(d3) = -19.25$ cm^{-1} ($J(d2)$ being 2 orders of magnitude smaller that the other two, which are almost identical). These interactions established among the radicals of the crystal define the corresponding magnetic topology that appears to be a nearly isotropic 2-leg spin-ladder in which the rails are due to d1 and the rungs to d3 (see Figure 5a). Adjacent ladders present a small $J(d2)$ interaction along the *c*-axis, and no magnetic contacts along the *b*-axis.

Previous studies on ionic crystals have shown that the Madelung field affects the electronic distribution of the anion-

(60) Johnston, D. C.; Troyer, M.; Miyahara, S.; Lidsky, D.; Ueda, K.; Azuma, M.; Hiroi, Z.; Takano, M.; Isobe, M.; Ueda, Y.; Korotin, M. A.; Anisimov, V. I.; Mahajan, A. V.; Miller, L. L. *Los Alamos National Laboratory, Preprint Archive, Condensed Matter;* Los Alamos National Laboratory: Los Alamos, NM, 2000; 1−63, arXiv:cond-mat/0001147.

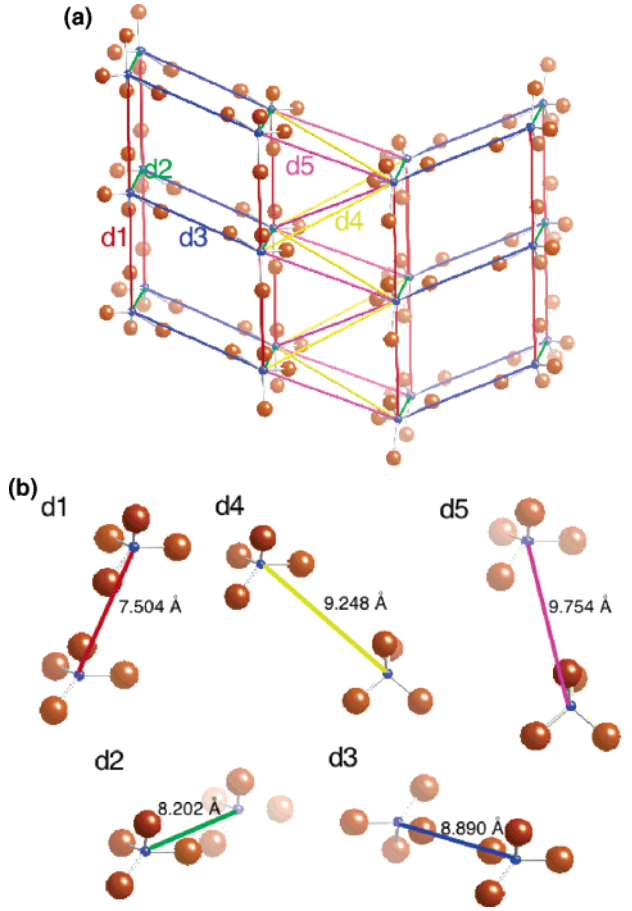

Figure 4. (a) Crystal packing in terms of $CuBr_4^{2-}$ radicals, where Cu···Cu distances shorter than 10.0 Å are shown. (b) Geometry of all unique radical−radical dimers found in the crystal. The Cu···Cu distance (in Å) is also given for each pair.

radicals and must be taken into account using and embedded cluster model.[61] This effect can be corrected by computing the energy of the radical−radical pairs in the presence of four nearby 2,3-dmpyH$^+$ cations (including the counterions mimics the real molecular environment of the $CuBr_4^{2-}$ anions within the crystal). There are many forms of selecting those four cations. Among all neutral (2,3-dmpyH$^+$)$_4$($CuBr_4^{2-}$)$_2$ models, we have selected those where the four 2,3-dmpyH$^+$ counterions established the shortest distances with their corresponding two $CuBr_4^{2-}$ anions. We thus obtained the J_{AB} values shown in the last column of Table 4. Notice there is a significant difference between J_{AB} values depending on whether the model used in the computation is anionic or neutral. When the counterions are included, all computed J_{AB} values become smaller in absolute value, a fact that leads d2 to be negligible. The magnetic topology using the anion$_2$cation$_4$ J_{AB} values is that of an *ideal* (isolated) 2-leg spin-ladder (Figure 5b). It follows that the strength of the magnetic exchange between Cu(II) atoms results from Br···Br contacts as well as 2,3-dmpyH$^+$···$CuBr_4^{2-}$ contacts.

The computation of the macroscopic properties (using the values of J_{AB} from column 5 of Table 4) requires a proper finite model of the crystal (the so-called, minimal magnetic model space). For an isolated 2-leg spin-ladder topology, we have found previously that a four site (4s) model that includes two rungs of the spin-ladder model and, thus, 4 radical $CuBr_4^{2-}$ units is the smallest model space.[42] Thus, we have done numerical simulations of $\chi(T)$ and $\chi T(T)$ using models of increasing size ranging from 4s (2-rung model) to 14s (7-rung model) in order to study the magnetic susceptibility curve for a spin-ladder magnetic topology. Figure 6 shows the computed magnetic susceptibility curves for several of these model spaces. We can conclude that an 8s model is an appropriate minimal magnetic model for (2,3-dmpyH)$_2$$CuBr_4$ crystal: (i) simulated $\chi(T)$ values using smaller 4s and 6s models converge to $\chi(T)$ computed using the 8s model; (ii) using larger 10s−14s models almost overlap those data computed using the 8s model. Figure 7 shows a direct comparison between the experimental and simulated (a) $\chi(T)$ and (b) $\chi T(T)$ data using the minimal 8s magnetic model. The agreement between experimental and computed curves is an indication of the quality of our simulations. Finally, the singlet−triplet spin-gap for the bulk system has been computed to be 12.47 K using the 8s model and 3.69 K in the extrapolated case of an infinite spin-ladder model.

Table 4. Value of J_{AB} Computed for Each Unique Radical−Radical Pair. The Shortest Cu···Cu and Br···Br Distances between the Radicals of the Pair Are Also Given.

dimers d*i*	*d*(Cu···Cu) [Å]	*d*(Br···Br)$_{min}$ [Å]	*J*(d*i*) [cm^{-1}] anion$_2$	*J*(d*i*) [cm^{-1}] anion$_2$cation$_4$
d1	7.504	3.905	−22.50	−7.79
d2	8.202	4.748	−0.22	0.00
d3	8.890	4.328	−19.25	−3.49
d4	9.248	6.428	<|0.1|	
d5	9.754	6.494	<|0.1|	

Discussion

It is well-known that halide−halide nonbonding contacts between CuX_4^{2-} ions propagate magnetic exchange interactions.[62−68] A number of parameters appear to affect the strength of the exchange, including the X···X distance, Cu−X···X angles and the Cu−X···X−Cu torsion angle.[56] Shorter X···X distances, larger Cu−X···X angles, and torsion angles near 0° and 180° correlate with larger antiferromagnetic exchange constants.

As mentioned above, from the structural point of view, nearest neighbor analysis of the Br···Br contacts in the crystal structure of **1** suggests that the compound should be a magnetic ladder. The crystal symmetry ensures that there is only one uniform magnetic exchange pathway along the rails and only one across the rails. The values in Table 2 indicate that the Br···Br distances along the rails of the ladder [3.905(1) Å] are significantly shorter than those forming the rungs [4.328(1) Å]. The Cu−Br···Br angles across the ladder rungs are 155.5(1)° (identical due to the inversion symmetry) and alternate down the rails between

(61) The original reference on embedded cluster models is given in Ellis, D. E.; Benesh, G. A.; Byrom, E. *Phys. Rev. B: Condens. Matter Mater. Phys.* **1977**, *16* (8), 3308−3313. For a recent application, see Fink, K. *Chem. Phys.* 2006, *326* (2−3), 297−307.

(62) Block, R.; Jansen, L. *Phys. Rev. B: Condens. Matter Mater. Phys.* **1982**, *26*, 148−153.
(63) Snively, L. O.; Haines, D. N.; Emerson, K.; Drumheller, J. E. *Phys. Rev. B: Condens. Matter Mater. Phys.* **1982**, *26*, 5245−5247.
(64) Straatman, P.; Block, R.; Jansen, L. *Phys. Rev. B: Condens. Matter Mater. Phys.* **1984**, *29*, 1415−1418.
(65) Marsh, W. E.; Hatfield, W. E.; Hodgson, D. J. *Inorg. Chem.* **1988**, *27*, 1819−1822.
(66) Whangbo, M. H.; Koo, H. J.; Dai, D.; Jung, D. *Inorg. Chem.* **2003**, *42*, 3898−3906.
(67) Willett, R. D.; Butcher, R.; Landee, C. P.; Twamley, B. *Polyhedron* **2005**, *24*, 2222−2231.
(68) Willett, R. D.; Twamley, B.; Montfrooij, W.; Granroth, G. G.; Nagler, S. E.; Hall, D. W.; Park, J.-H.; Watson, B. C.; Meisel, M. W.; Talham, D. R. *Inorg. Chem.* **2006**, *45*, 7689−7697.

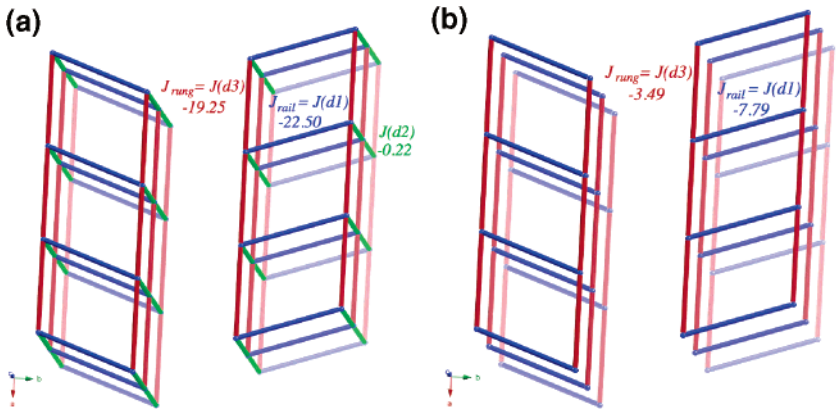

Figure 5. Magnetic topology of the crystal obtained in terms of the computed J_{AB} parameters (in cm^{-1}): (a) using isolated $anion_2$ radical−radical pairs; (b) using $anion_2cation_4$ clusters.

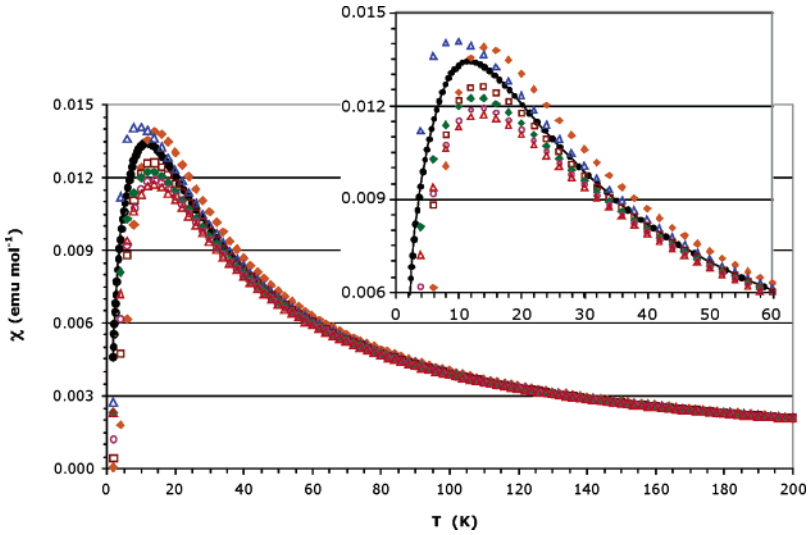

Figure 6. Computed magnetic susceptibility curves using various models of increasing size: 4s (red diamond), 6s (blue triangle), 8s (square), 10s (green diamond), 12s (circle), and 14s (red triangle). The experimental curve is also given for comparison (filled circle).

151.0(1)° and 127.6(1)°. Torsion angles along both pathways are near the optimal values: −2.0(1)° for the rails and 180° for the rungs. Therefore, it was expected that the rail magnetic exchange would be larger than the rung exchange. The J'_{rail} and J'_{rung} values obtained when fitting the magnetic susceptibility curve to a strong-rail model (−6.02 and −3.10 cm^{-1}, respectively) agree well with these expectations. Theoretical studies confirmed the *ideal* (isolated) 2-leg spin-ladder magnetic topology of the crystal at 88 K and found values for the J_{rail} and J_{rung} of −7.79 and −3.49 cm^{-1}. These computed J_{AB} should be thus compared to previously fitted −6.02 and −3.10 cm^{-1}, respectively, which compare well.

Analysis of the magnetic susceptibility of **1** has shown it to behave as a second example of a *strong rail* ladder in which J_{rung} is weaker than J_{rail}; for **1**, the J_{rung}/J_{rail} ratio is 0.52 based on the magnetic data or 0.45 according to the theoretical calculations. Only *bis*cyclopentylammonium tetrabromocuprate[22] has previously been reported as a strong rail ladder with $J_{rung}/J_{rail} = 0.45$.

As mentioned above, previous studies of $(VO)_2(P_2O_7)$ and Cu_2(1,4-diazacycloheptane)Cl_4 concluded that they were strong *rung* spin-ladders, based on crystal structures and susceptibility data. However, further investigations indicated that both compounds indeed had singlet ground states, but the energy gaps were due to the presence of a magnetic alternating chain[29,30] in $(VO)_2(P_2O_7)$ and to the presence of multiple antiferromagnetic interactions in Cu_2(1,4-diazacycloheptane)Cl_4.[34,35] It is now recognized that the susceptibilities as a function of temperature of a strong-rung spin-ladder and an alternating chain can be identical, although for different combinations of parameters. Therefore, the use of only magnetic susceptibility and structural data can lead to the wrong conclusion. This is why we have applied the first-principles, bottom-up approach to support our magnetic topology. This procedure has been shown to work well in other two-leg spin-ladder systems.[19] Also, let us point out that there is less risk of misinterpretation for the study of **1** owing to its strong-rail nature. A further indication of a two-leg spin-ladder is the presence of a spin gap. The energy gap is due to the presence of J_{rung} but, for equal rung interaction strengths, the energy gap of a strong rail ladder is significantly smaller than that of a strong rung ladder. Evidence for a small energy gap in **1** is seen in the low-temperature susceptibility data (insert of Figure 3) that continues to decrease at lower temperatures with an increasing slope even at the lowest measured temperature. For temperatures less than the gap energy, the susceptibility initially increases rapidly with positive curvature as $\chi \propto \exp(-\Delta/kT)/T$.[69] Since the susceptibility of **1** is displaying negative curvature with temperature, even at 1.8

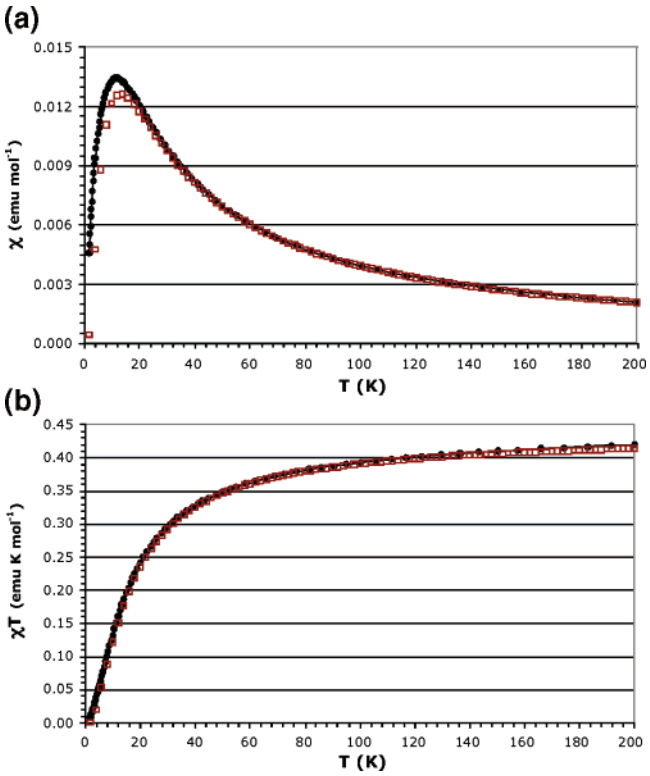

Figure 7. Shape of the computed (a) $\chi(T)$ and (b) $\chi T(T)$ curves using the minimal 8s magnetic model (red squares). The experimental curve is also given (filled circle).

K, we conclude the energy gap can be as large as 2 K. The computed singlet−triplet spin-gap has been extrapolated to be 3.69 K and compares well with the experimental energy gap, which ranges from 1.5 to 4 K.[70] The computed energy gap is slightly larger than the experimental one. This could be due to various factors, probably the most relevant being the use of 88 K crystal-structure data to compute the gap, while the measured value is obtained at a much lower temperature.

(69) Troyer, M.; Tsunetsugu, H.; Wuertz, D. *Phys. Rev. B: Condens. Matter Mater. Phys.* **1994**, *50* (18), 13515−13527.
(70) Further, experiments confirm the existence of a small gap. Low-temperature magnetization studies of **1** found the lower critical field to be near 2.5 tesla, indicating a gap energy of approximately 1.5 K. In addition, inelastic neutron scattering experiments on a partially deuterated crystal of **1** found an energy gap near 4 K. The range of experimental values for the gap is not yet understood.
(71) Broholm, C.; Hong, T. Unpublished results.

Conclusions

We have prepared the second example of a two-leg, strong-rail antiferromagnetic spin-ladder and characterized its magnetic behavior [experimental: $J_{rung} = -3.10$ cm^{-1}, $J_{rail} = -6.02$ cm^{-1}. Calculated: $J_{rung} = -3.49$ cm^{-1}, $J_{rail} = -7.79$ cm^{-1}]. This conclusion is supported by the crystal structure, magnetic data, and theoretical calculations all of which suggest that the only significant magnetic exchange interactions in the sample are those that constitute the rails and rungs appropriate to a two-leg spin-ladder model. Agreement for the exchange interactions and powder susceptibility between the theoretical calculations and experimental data is compelling and shows the utility of the new first principles bottom-up work strategy for calculating bulk physical properties from molecular structure. The small disagreement between the theoretical and experimental predictions of the spin gap energy requires further study. Preliminary neutron scattering measurements on **1** indicate that the compound fits the two-leg spin-ladder model with the ladder extending along the crystallographic *a*-axis, in agreement with the calculations and magnetic susceptibility measurements.[71] Further neutron scattering data will be needed for final experimental confirmation of these conclusions and a better experimental measurement of the spin gap.

Acknowledgment. The U.S. team is grateful for grants from the NSF (Grant IMR-0314773) toward the purchase of the MPMS SQUID, from PCISynthesis Inc. toward the purchase of the D8 powder X-ray diffractometer, and from the Kresge Foundation toward the purchase of both. Summer support for A.S. through an Albert C. Erickson Summer Fellowship is gratefully acknowledged. The team from Universitat de Barcelona also thanks the Spanish Science and Education Ministry for support (Projects BQU2002-04587-C02-02 and CTQ2005-02329), the Catalan DURSI (Grants 1999SGR-00046 and 2005SGR-00036), and the computer time allocated by CESCA and BSC. M.D. thanks the Spanish Science and Education Ministry for the award of a "Ramón y Cajal" Fellowship.

Supporting Information Available: Crystallographic data in CIF format. This material is available free of charge via the Internet at http://pubs.acs.org.

JA066330M